Traveling solitons in the parametrically driven nonlinear Schrödinger equation

I. V. Barashenkov,* E. V. Zemlyanaya,† and M. Bär‡
Max-Planck-Institut für Physik komplexer Systeme, Nöthnitzer Strasse 38, Dresden, Germany
(Received 19 June 2000; published 14 June 2001)

We show that the (undamped) parametrically driven nonlinear Schrödinger equation has wide classes of traveling soliton solutions, some of which are stable. For small driving strengths stable nonpropagating and moving solitons co-exist while strongly forced solitons can only be stable when moving sufficiently fast.

DOI: 10.1103/PhysRevE.64.016603 PACS number(s): 05.45.Yv, 05.45.Xt

I. INTRODUCTION

The parametrically driven damped nonlinear Schrödinger (NLS) equation,

$$i\psi_t+\psi_{XX}+2|\psi|^2\psi-\psi=h\psi^*-i\gamma\psi, \tag{1}$$

was used to model the nonlinear Faraday resonance in a vertically oscillating fluid layer [1,2] and the effect of phase-sensitive parametric amplifiers on solitons in optical fibres [3]. The same equation describes an easy-plane ferromagnet with a combination of a static and high frequency field in the easy plane [4,5]. It also serves as a continuum limit for small-amplitude excitations in the parametrically driven Frenkel-Kontorova chain (an array of diffusively coupled pendula) [6]. The Frenkel-Kontorova system is regarded as a fairly realistic model of a number of physical and biophysical systems and phenomena, including ladder networks of discrete Josephson junctions, charge-density wave conductors, crystal dislocations in metals, DNA dynamics and proton conductivity in hydrogen-bonded chains [7].

The second term in the right-hand side of Eq. (1) accounts for dissipative losses that occur in all physical systems but are frequently ignored on short time intervals. To compensate for these losses, one has to pump the energy into the system from outside. The first term in the right-hand side of Eq. (1) represents one possible way of pumping the energy in, the parametric pumping. In the absence of the damping and pumping, the nonlinear Schrödinger equation exhibits soliton solutions that can travel with arbitrary velocities and transport physical characteristics such as mass, momentum and energy. [For the sake of brevity, we are making use of the hydrodynamical interpretation of Eq. (1) here.] The dissipation has two visible effects on the soliton: it attenuates its speed and damps its amplitude. The parametric driving is well known to be capable of counterbalancing the damping of the soliton's amplitude; a natural question now is whether it can sustain its motion with a nonzero velocity.

In fact the existence of traveling solitons is a nontrivial matter even in the absence of damping. The driving term $h\psi^*$ in

$$i\psi_t+\psi_{XX}+2|\psi|^2\psi-\psi=h\psi^* \tag{2}$$

breaks the Galilean invariance of the unperturbed nonlinear Schrödinger equation and hence one cannot obtain a moving soliton simply by boosting a static one. However the Galilean or Lorentz symmetry is not always a prerequisite for the existence of moving nonlinear waves. For example, reaction-diffusion equations do not possess any symmetries of this kind but are well known to support stably propagating fronts and pulses (whose velocities are fixed by parameters of the model.) In particular, traveling domain walls arise in the parametrically driven Ginsburg-Landau equations (where the motion is due to nongradient terms) [8]. As far as solitons in Hamiltonian systems are concerned, the example of dark solitons in the nonlinear Schrödinger equations suggests that they have even a greater mobility than dissipative fronts and pulses. Although in this case the Galilean invariance is broken by the presence of the nonzero background, the dark solitons can propagate with arbitrary speeds bounded only by the velocity of sound waves [9–12].

A number of nonstationary regimes were reported in the water tank experiments, including the formation of oscillating soliton pairs [2], but no steadily moving solitons were detected so far. On the other hand, numerical simulations of the undamped equation (2) did exhibit traveling localized objects [13]. It has remained an open question whether these moving objects preserve their speed and amplitude, or attenuate and decay slowly due to the emission of the second-harmonic radiation. The aim of the present paper is to study the existence of steadily propagating solitons, and examine their stability. Here we are confining ourselves to the undamped situation relegating the analysis of the effect of damping to future publications.

In addition to their role in transport phenomena, stably moving solitons are also of interest as alternative attractors that may compete with (static or oscillating) nonpropagating solutions. We will demonstrate that stable traveling solitons do exist in the (undamped) parametrically driven nonlinear Schrödinger equation. Moreover, there are parameter ranges where moving solitons are stable whereas their quiescent counterparts are not. Unstable solitons are not meaningless either; they may arise as long-lived transients and intermediate states in spatiotemporal chaotic regimes. In this paper we

*On leave from Department of Mathematics, University of Cape Town, Private Bag, Rondebosch 7701, South Africa. Email address: igor@cenerentola.mth.uct.ac.za

†On leave from the Laboratory for Computing Techniques, Joint Institute for Nuclear Research, Dubna, 141980, Russia. Email address: elena@ultra.jinr.ru

‡Email address: baer@mpipks-dresden.mpg.de

will identify oscillatory and translational instabilities of traveling solitons and simulate their nonlinear evolution near the transition curves.

The structure of the paper is as follows. In Sec. II we derive an *a priori* bound for the existence domain of traveling solitons and introduce the linearized eigenvalue problem for their stability analysis. We also discuss some general properties of eigenvalues and eigenfunctions and formulate a simple criterion for the onset of the nonoscillatory instability: $\partial P/\partial V=0$, where V is the velocity of the steadily moving soliton, and P the associated momentum.

In Sec. III we present several explicit quiescent ($V=0$) solutions and then derive the necessary condition for a static solution to be continuable to nonzero velocities. This condition requires that the motionless solution should either not have any ''free'' parameters apart from the translational shift, or, if there is an additional parameter z, the equation $\partial P/\partial z=0$ should be satisfied. Here P is the momentum of the motionless localized solution (which, contrary to one's mechanical intuition, is not necessarily equal to zero). There are three static solutions satisfying the above condition, two of which being the well-known constant-phase ψ_+ and ψ_- solitons, respectively, while the third solution looks like a pulse with a bell-shaped modulus and twisted phase.

The most important results of this work are contained in Sec. IV where we report on the numerical continuation of various branches of solutions and their stability analysis. In agreement with the analytical predictions of the preceding section, we find that each of the above static solutions admits the continuation to nonzero V. The stability properties of traveling solitons result from an intricate interplay of two types of instabilities, the oscillatory and translational instability. In accordance with the conclusions of Sec. II, the numerical analysis of the linearized eigenvalues shows that the transition curves of the translational instability satisfy $\partial P/\partial V=0$. One interesting conclusion of the stability analysis is that although quiescent solitons are unstable for driving strengths larger than $h=0.064$, there are stable moving solitons for any $0\leqslant h\leqslant 1$. We discuss in detail the soliton's transformation as it is continued in V, paying special attention to the dynamics of the associated linearized eigenvalues on the complex plane. Two different scenarios of the transformation are identified, one occurring for small h and the other one for larger driving strengths, and we also describe an interesting crossover from one to another.

Section V is devoted to the direct numerical simulations of the full time-dependent nonlinear Schrödinger equation. We show that the evolution of both types of the soliton instabilities leads, as $t\to\infty$, to the same asymptotic attractors. Finally, Sec. VI summarizes conclusions of this study.

II. STEADILY TRAVELING WAVES: EXISTENCE AND STABILITY

A. Existence domain

We will confine ourselves to localized traveling waves of the simplest form, $\psi(X,t)=\psi(X-Vt)$. Transforming to the comoving frame, these correspond to time-independent soliton solutions of the equation

$$i\psi_t - iV\psi_x + \psi_{xx} + 2|\psi|^2\psi - \psi = h\psi^*, \tag{3}$$

where $x=X-Vt$. We will search for these static solutions by solving an ordinary differential equation

$$-iV\psi_x + \psi_{xx} + 2|\psi|^2\psi - \psi = h\psi^* \tag{4}$$

under the vanishing boundary conditions $|\psi(x)|\to 0$ as $|x|\to\infty$. Here h is always taken positive; negative h's can be recovered by the phase transformation $\psi\to i\psi$.

It is straightforward to notice that if the function $\psi(x)$ describes a soliton traveling with the velocity V, the functions $\psi^*(x)$ and $\psi(-x)$ yield solitons moving with the velocity $-V$. Therefore, either the function $\psi(x)$ satisfies $\psi^*(x)=\pm\psi(-x)$ (that is, one of the real and imaginary part of the solution is even and the other one odd), or there are two solutions associated with the same V. (Here we are not making any difference between solutions that are different just in the overall sign.) In the latter case the solutions will not exhibit the $\psi^*(x)=\pm\psi(-x)$ symmetry. We will try to restrict ourselves to positive V's wherever possible; negative velocities will only be presented where this may help visualizing how different branches of solutions are connected.

Next, it is easy to show that solitons cannot travel faster than a certain speed limit. Indeed, as $|x|\to\infty$, the soliton's asymptotic tail decays as $\psi(x)\sim e^{-\kappa x}$, where

$$2\kappa^2 = 2 - V^2 \pm \sqrt{(2-V^2)^2 + 4(h^2-1)}. \tag{5}$$

Large driving strengths $h>1$ are of little interest to us as in this case the zero background, $\psi(x)=0$, is unstable with respect to continuous spectrum waves [5]. Therefore we are not going to discuss this case here. In the complementary region $h<1$, the location of κ on the complex plane depends on the value of the velocity. When $V^2<2-2\sqrt{1-h^2}$, there are four real exponents; for $2-2\sqrt{1-h^2}<V^2<c^2$, where

$$c=\sqrt{2+2\sqrt{1-h^2}}, \tag{6}$$

we have a quadruplet of complex κ's. Finally, for $V^2>c^2$ all four exponents are imaginary. Consequently, there can be no exponentially localized solitons traveling faster than c. Physically, c represents the minimum phase velocity of linear waves governed by Eq. (1), and our condition $V<c$ is essentially an exclusion principle ruling out a resonance between solitons and linear waves.

B. Linearized eigenvalue problem

In this paper we solve the Eq. (4) numerically and examine the stability of the resulting solutions by studying the associated eigenvalue problem. This eigenvalue problem arises by assuming a small perturbation of the form

$$\delta\psi(x,t)=y(x)e^{\lambda t}, \quad y(x)=\delta u(x)+i\,\delta v(x).$$

Substituting into Eq. (3) gives

$$\mathcal{H}Y=\lambda JY, \tag{7}$$

where the Hermitian operator $\mathcal{H}$ has the form

$$\mathcal{H}=I(-\partial_x^2+1)+VJ\partial_x + \begin{pmatrix} h-6u^2-2v^2 & -4uv \\ -4uv & -h-6v^2-2u^2 \end{pmatrix}, \tag{8}$$

the matrix J is given by

$$J=\begin{pmatrix} 0 & -1 \\ 1 & 0 \end{pmatrix}, \tag{9}$$

and the column vector $Y(x)=(\mathrm{Re}\,y,\mathrm{Im}\,y)^T=(\delta u,\delta v)^T$. In Eq. (8) I is the identity matrix, and we have decomposed the stationary solution as $\psi(x)=u(x)+iv(x)$.

For symmetric solutions satisfying $\psi^*(x)=\pm\psi(-x)$, eigenvalues will always come in $(\lambda,-\lambda)$ pairs. This follows from the fact that for these solutions changing $x\to -x$ in the operator (8) amounts to changing the sign of its off-diagonal elements, and hence if $[\delta u(x),\delta v(x)]^T$ is an eigenfunction associated with an eigenvalue λ, the column $[\delta u(-x), -\delta v(-x)]^T$ will serve as an eigenfunction associated with an eigenvalue $-\lambda$. As far as a zero eigenvalue is concerned, it will have a twin with the eigenfunction $[\delta u(-x), -\delta v(-x)]^T$ unless its eigenfunction $y=\delta u+i\,\delta v$ satisfies the symmetry $y^*(x)=e^{i\varphi}y(-x)$, where $\varphi=\mathrm{const}$.

To complete the discussion of the spectrum structure, we need to mention that there are two branches of the continuous spectrum lying on the imaginary axis of λ: $\lambda=i\omega_{1,2}(k)$, where

$$\omega_{1,2}(k)=Vk\pm\sqrt{(k^2+1)^2-h^2},$$

and $-\infty<k<\infty$. (We are still assuming $h<1$). In the region $V^2<c^2$, which is of interest to us, the continuous spectrum has a gap: $\omega_1(k)>\omega_0$, $\omega_2(k)<-\omega_0$, where $\omega_0>0$. This gap can harbor discrete eigenvalues representing stable oscillation modes.

C. Nonoscillatory instabilities

The aim of this subsection is to demonstrate that a pair of pure imaginary eigenvalues can collide at $\lambda=0$ and move onto the real axis only at the velocity satisfying $\partial P/\partial V=0$, where

$$P=\frac{i}{2}\int(\psi_x^*\psi-\psi_x\psi^*)dx \tag{10}$$

is the conserved momentum. This criterion is known in the context of dark solitons of the undriven nonlinear Schrödinger equations; see [10–12]. Here we simply adapt the proof given in [11] to the case of the equation with the parametric forcing. An important assumption that we make here, is that the solution whose stability is being examined, does not have any free parameters apart from the trivial translation parameter x_0.

First of all we need to make a remark on the integrable case, $h=0$. In this case solutions of the ordinary differential equation (4) can be obtained from a quiescent soliton of Eq. (2) by a Galilei transformation,

$$\psi(x)=e^{i(V/2)x}A\,\mathrm{sech}\,Ax, \tag{11}$$

where $A=\sqrt{1-V^2/4}$. For $h=0$ and any $|V|<2$, the linearized operator $\mathcal{H}$ has four zero eigenvalues associated with two eigenvectors. One of these eigenvectors originates from the translation symmetry and the other one results from the phase invariance of Eq. (4). The term $h\psi^*$ breaks the phase invariance and hence as h is increased from zero, one pair of eigenvalues $(\lambda,-\lambda)$ moves away from the origin on the complex plane. As h and V are further varied, a pair of eigenvalues may return to the origin. If the solution of Eq. (4) at the point of their return is a member of a family parametrized by *two* free parameters, we will have, again, four zero eigenvalues with two eigenfunctions. (The eigenfunctions are simply derivatives of the solution with respect to the free parameters.) Our analysis will not be applicable in this case, and the equality $\partial P/\partial V=0$ does not have to be valid at the return point. (We will come across this type of a situation in Sec. IV C below.) However, a more common situation is when the solution at the return point is a member of a *one*-parameter family. We will show that in this case the relation $\partial P/\partial V=0$ does have to be in place.

Let us denote V_c the velocity for which the eigenvalue of the operator (7)–(8) vanishes. We can develop the solution $\psi(V;x)$ in powers of $\epsilon=V-V_c$,

$$\psi(V;x)=\psi_0(x)+\epsilon\psi_1(x)+\epsilon^2\psi_2(x)+\cdots,$$

where $\psi_0=\psi(V_c;x)$. Accordingly, the operator $\mathcal{H}$ expands as $\mathcal{H}=\mathcal{H}_0+\epsilon\mathcal{H}_1+\epsilon^2\mathcal{H}_2+\ldots$. If the eigenvalue λ moves from imaginary to the real axis, it is natural to assume that it admits an expansion of the form

$$\lambda=\epsilon^{1/2}\lambda_1+\epsilon^{3/2}\lambda_3+\epsilon^{5/2}\lambda_5+\cdots. \tag{12}$$

The associated eigenfunction is then developed as

$$Y(x)=Y_0(x)+\epsilon^{1/2}Y_1(x)+\epsilon Y_2(x)+\cdots. \tag{13}$$

When $\epsilon=0$, we have $\mathcal{H}_0Y_0=0$, i.e., Y_0 is a null eigenvector at the bifurcation point $V=V_c$. Since we have assumed that $\psi(V_c,x)$ is a member of a one-parameter family of solutions, the operator $\mathcal{H}_0$ has only one null eigenvector, and we have to identify $Y_0=\Psi_0'(x)$. Here Ψ_0 is a column vector formed by the real and imaginary part of the soliton ψ_0: $\Psi_0=(u_0,v_0)^T$. The prime indicates differentiation with respect to x.

Next, setting the coefficient of $\epsilon^{1/2}$ to zero yields

$$\mathcal{H}_0Y_1=\lambda_1JY_0.$$

Comparing this to the equation

$$\mathcal{H}_0\frac{\partial\Psi}{\partial V}\bigg|_{V=V_c}=-J\Psi_0',$$

which arises from the differentiation of Eq. (4) with respect to V, we get

$$Y_1(x) = -\lambda_1 \left. \frac{\partial \Psi}{\partial V} \right|_{V=V_c}.$$

[In the above equations $\Psi = (u,v)^T$.] The coefficient of ϵ^1 produces

$$\mathcal{H}_0 Y_2 = \lambda_1 J Y_1 - \mathcal{H}_1 Y_0,$$

which has bounded solutions if the right-hand side is orthogonal to the null eigenvector of $\mathcal{H}_0$,

$$\lambda_1 \int Y_0 J Y_1 dx - \int Y_0 \mathcal{H}_1 Y_0 dx = 0. \tag{14}$$

The second term in Eq. (14) is readily shown to vanish—one only needs to expand the identity $\mathcal{H}\Psi' = 0$ in ϵ. (The coefficient of ϵ^1 gives $\mathcal{H}_1 \Psi_0' = -\mathcal{H}_0 \Psi_1'$. Taking the scalar product with Ψ_0' yields the required $\int \Psi_0' \mathcal{H}_1 \Psi_0' dx = 0$.) On the other hand, the first term in Eq. (14) is equal to $(\lambda_1^2/2)\partial P/\partial V$. Consequently, Eq. (14) gives either $\partial P/\partial V = 0$ or $\lambda_1 = 0$. If we assume that $\lambda_1 = 0$, we will not be able to conclude that $\partial P/\partial V = 0$ at this order of the expansion. However, the order ϵ^2 will then give us $\lambda_2^2 \partial P/\partial V = 0$, which implies either $\partial P/\partial V = 0$ or $\lambda_2 = 0$. Proceeding by a similar token we will eventually arrive at the equation $\partial P/\partial V = 0$ at some order ϵ^n where n is such that $\lambda_n \neq 0$. (Alternatively, we will have to conclude that all $\lambda_n = 0$ and hence we are dealing with a symmetry eigenvalue that is equal to zero for *all* V.)

Thus a pair of real or pure imaginary eigenvalues of the same magnitude and opposite sign, can only collide for the value of V that satisfies $\partial P/\partial V = 0$. Here we wish to reemphasize that we have obtained this conclusion under the assumption that the geometric multiplicity of the zero eigenvalue is *not* increased at the point of collision. A simple example when this assumption is not valid, is furnished by the case $h = 0$. In this case the momentum corresponding to the soliton (11) is given by $P = V\sqrt{1 - V^2/4}$. Although P has a maximum for $V = \sqrt{2}$, the stability properties of the undriven soliton do not change at this point. The reason is that for each V the operator $\mathcal{H}$ has two null eigenvectors in this case, and hence we cannot make the identification $Y_0 = \Psi_0'$. (Instead, Y_0 will be a linear combination of *two* zero modes.) Consequently, the above proof becomes invalid.

Finally, one can easily check that the above result does not really depend on how the eigenvalue λ expands in powers of ϵ. We assumed that the expansion (12) starts with terms of order $\epsilon^{1/2}$. This assumption is natural and supported by the numerical evidence; however, even if we had postulated the expansion starting with terms of order $\epsilon^{1/4}$, $\epsilon^{1/3}$ or say, ϵ, we would have still arrived at the *same* necessary condition for the zero crossing: $\partial P/\partial V = 0$.

The condition $\partial P/\partial V = 0$ admits a simple interpretation in terms of two integrals of motion. In addition to the momentum, Eq. (3) conserves the energy,

$$E = \mathrm{Re} \int (|\psi_x|^2 + |\psi|^2 - |\psi|^4 + h\psi^2) dx. \tag{15}$$

The stationary equation (4) can be regarded as a condition that the energy (15) be stationary under the fixed P: $(\delta E)_P = 0$ or, equivalently, $\delta(E - VP) = 0$, where V is the Lagrange multiplier. The relation $\delta E = V \delta P$ implies that the functions $E(V)$ and $P(V)$ have extrema at the same point $V = V_c$ and so there are two values of E corresponding to the same P. In other words, to each value of the momentum there correspond solitons with two different energies. Therefore, the instability of one of the two branches of solitons separated by the point V_c with $\partial P/\partial V = 0$, can be interpreted as the instability against the decay into a soliton of the other branch and a symmetric radiation (which takes away the energy difference but does not affect the momentum.)

III. QUIESCENT SOLUTIONS AND CONTINUATION TO $V \neq 0$

In order to continue in V we need to have some ''starting points'' at $V = 0$. Two such quiescent solutions of Eq. (4) are well known:

$$\psi_+(x) = A_+ \,\mathrm{sech}(A_+ x), \tag{16a}$$

$$\psi_-(x) = iA_- \,\mathrm{sech}(A_- x), \tag{16b}$$

where $A_\pm^2 = 1 \pm h$. The soliton ψ_- is unstable with respect to a nonoscillatory mode for all h while the ψ_+ is stable for $h < h_0 = 0.063\,596$ and develops an oscillatory instability as h is increased beyond h_0 [5]. In this section we will show that both ψ_+ and ψ_- are continuable to $V \neq 0$, and identify another continuable solution.

A. The ''twist'' soliton

Writing $\psi = u + iv$, the stationary equation (4) transforms into the system

$$u_{xx} - u - hu + 2u(u^2 + v^2) = 0, \tag{17}$$

$$v_{xx} - v + hv + 2v(u^2 + v^2) = 0. \tag{18}$$

The system (17) and (18) appeared previously in connection with light pulses in a birefringent optical fibre. Using Hirota's approach, Tratnik and Sipe [14] obtained the following exact solution to Eqs. (4),(17) and (18):

$$\psi = \psi(z;x) = u + iv, \tag{19a}$$

$$u = 2A_+ e^{\theta_2} D^{-1} (1 + e^{2(\theta_1 - \beta)}), \tag{19b}$$

$$v = 2A_- e^{\theta_1} D^{-1} (1 - e^{2(\theta_2 - \beta)}), \tag{19c}$$

where

$$D = 1 + e^{2\theta_1} + e^{2\theta_2} + e^{2(\theta_1 + \theta_2 - 2\beta)},$$

$$\theta_1 = A_-(x - z), \quad \theta_2 = A_+(x + z);$$

the constant

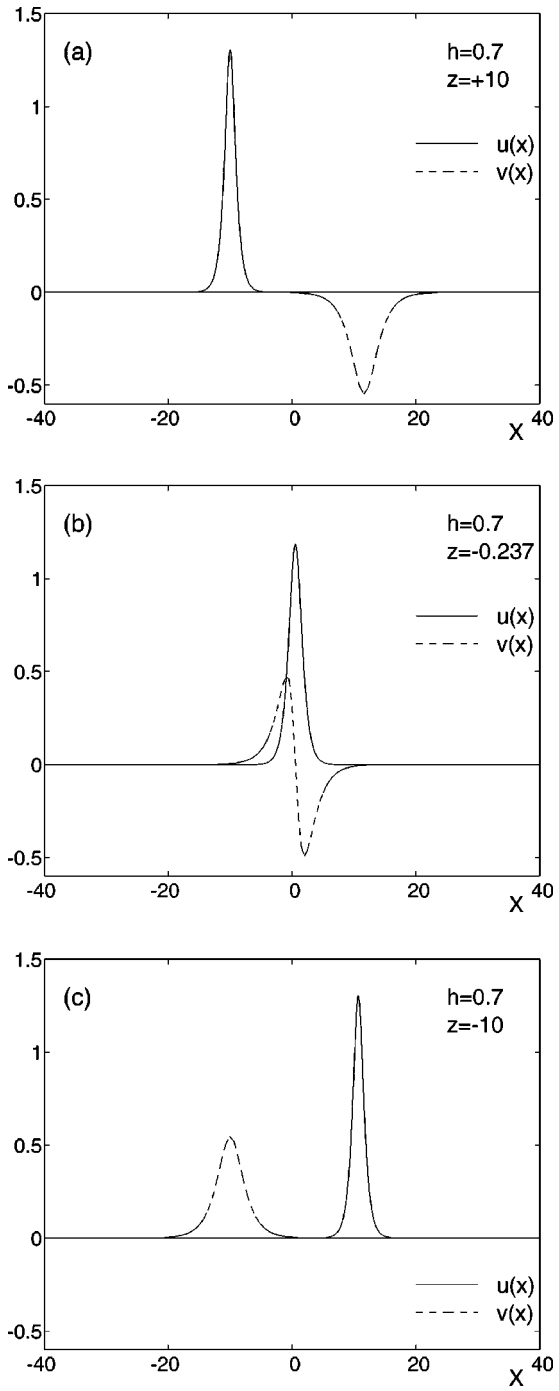

FIG. 1. Solution (19) for various z. (a) $z=10$; (b) $z=\zeta$ with ζ as in Eq. (22) (the twist soliton); (c) $z=-10$. Solid curve: real part; dashed line: imaginary part.

$$\beta=\frac{1}{2}\ln\left(\frac{A_+ + A_-}{A_+ - A_-}\right)>0; \tag{20}$$

the amplitudes $A_\pm$ are as in Eq. (16): $A_\pm=\sqrt{1\pm h}$, and z is a real parameter that can take arbitrary values. The solution (19) with $z=10$ and -10 is plotted in Figs. 1(a)–1(c). As is clear from the figure, for sufficiently large $|z|$ the solution represents a complex of two solitons, ψ_+ and ψ_-, with the separation equal to approximately $2|z|$.

It is useful to notice a simple relation between two solutions of the form (19)—one with the parameter value $z=\zeta+\xi$ and the other one with $z=\zeta-\xi$:

$$\psi(\zeta+\xi;\eta-y)=\psi^*(\zeta-\xi;\eta+y). \tag{21}$$

Here ζ and η are defined by the driving strength h,

$$\zeta=-\frac{\beta}{2}\left(\frac{1}{A_-}-\frac{1}{A_+}\right)<0 \tag{22}$$

and

$$\eta=\frac{\beta}{2}\left(\frac{1}{A_-}+\frac{1}{A_+}\right), \tag{23}$$

while ξ and y can take arbitrary values. The relation (21) implies that the solution (19) with $z=\zeta$ is symmetric about the point $x=\eta$,

$$\psi(\zeta;\eta-y)=\psi^*(\zeta;\eta+y). \tag{24}$$

That is, the real part of this solution is even and imaginary part odd with respect to $x=\eta$,

$$u(\eta-y)=u(\eta+y), \quad v(\eta-y)=-v(\eta+y).$$

[See Fig. 1(b).] This particular representative of the family (19) will play a special role in what follows. Similarly to the solitons ψ_+ and ψ_-, the modulus of the symmetric solution is bell shaped, but, unlike the constant phase of the ψ_+ and ψ_-, its phase changes by π as x varies from $x=-\infty$ to $x=\infty$. The solution looks like a pulse twisted by 180° in the (u,v) plane. For this reason we will be referring to solution (19) with $z=\zeta$ as the ''twist'' soliton.

For $h=\frac{3}{5}$ the ''twist'' acquires a particularly simple form. In this case Eq. (22) gives $\zeta=-(1/8)\sqrt{5/2}\ln 3$. Substituting in Eqs. (19) and shifting the resulting solution by $x_0=3z$, we get

$$u_T=\sqrt{\frac{6}{5}}\,\mathrm{sech}^2\,\tilde{x}; \quad v_T=\pm\sqrt{\frac{6}{5}}\,\mathrm{sech}\,\tilde{x}\,\tanh\,\tilde{x}, \tag{25}$$

where $\tilde{x}=\sqrt{\frac{2}{5}}x$. [The soliton (25) can also be obtained by a more direct method [15].]

B. The moving soliton bifurcation

Suppose the equation (4) has a one-parameter family of quiescent solutions $\psi(z;x)$. Here z can be any nontrivial parameter; the only requirement is that z should not be just an overall shift in x. One such family is given by Eq. (19) and there can also be other families for which ψ is not available explicitly. We will show in this section that in order for a solution with some $z=z_0$ to be continuable to nonzero V, the corresponding momentum integral should satisfy

$$\left.\frac{\partial P}{\partial z}\right|_{z=z_0}=0. \tag{26}$$

Let us assume that Eq. (4) with $V\neq 0$ has a solution $\psi(x)$, and that this solution is an analytic function of V in some neighborhood of $V=0$. Then we can expand it in the Taylor series

$$\psi(x)=\psi_0(x)+V\psi_1(x)+V^2\psi_2(x)+\cdots, \tag{27}$$

where $\psi_0(x)=\psi(z_0;x)=u_0+iv_0$ is some representative of the family of ''motionless'' solutions $\psi(z;x)$ with the parameter value z_0. Substituting Eq. (27) into Eq. (4) and equating coefficients of like powers of V, we get, at the order V^1:

$$\mathcal{H}\begin{pmatrix} u_1 \\ v_1 \end{pmatrix}=J\partial_x\begin{pmatrix} u_0 \\ v_0 \end{pmatrix}. \tag{28}$$

Here $u_1+iv_1=\psi_1$ and the operator $\mathcal{H}$ is given by Eq. (8). Equation (28) is solvable in the class of square integrable functions if the vector in the right-hand side is orthogonal to all homogeneous solutions, i.e., to all null eigenvectors of the operator $\mathcal{H}$. Since there is a family of ''motionless'' solutions parametrized by z and by an arbitrary spatial shift x_0 (which we have disregarded so far), the operator $\mathcal{H}$ has two zero modes. One is the translation mode $\partial_x\psi_0=\partial_x(u_0+iv_0)$; the corresponding solvability condition is trivially satisfied,

$$\int \partial_x(u_0,v_0)J\partial_x\begin{pmatrix} u_0 \\ v_0 \end{pmatrix}dx=0.$$

The other zero mode is given by the derivative $\partial_z\psi_0=\partial_z u_0+i\partial_z v_0$. The associated solvability condition reads

$$0=\int (\partial_z u_0,\partial_z v_0)J\partial_x\begin{pmatrix} u_0 \\ v_0 \end{pmatrix}dx=-\frac{1}{2}\frac{\partial P}{\partial z},$$

where P is the momentum integral (10). Consequently, a solution with nonzero V can only detach from the $V=0$ branch at the point where $\partial P/\partial z=0$.

Coming back to our explicit solutions, the ψ_+ and ψ_- solitons do not have any free parameters apart from the trivial position shift. Consequently, both solutions are continuable to nonzero V. Next, we have a family of solitonic complexes (19) with a nontrivial parameter z. As one can easily check, the momentum of the complex (19) as a function of z has a single minimum for some finite $z=z_0$ and tends to zero as $z\to\pm\infty$. To find z_0, we notice that the relation (21) implies

$$P(\zeta+\xi)=P(\zeta-\xi).$$

This means that the function $P(z)$ is even with respect to the point $z=\zeta$ and therefore, ζ is the point of the minimum: $z_0=\zeta$. Thus, the only representative of the family of the two-soliton complexes (19) that can be continued to nonzero V, is our twist soliton, $\psi(\zeta;x)$. [To be more precise, there are *two* twist solutions, one with positive and the other one with negative momentum. This is related to the fact that when $V=0$, we can generate new solutions to the system (17) and (18) by changing the sign of just one component, u or v.]

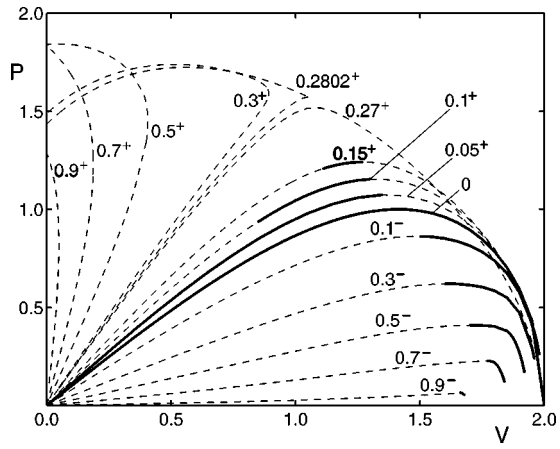

FIG. 2. The momentum of the ψ_+ and ψ_- solitons as a function of their velocities. Solid, dashed lines depict stable, unstable solutions, respectively. Decimal fractions attached to branches mark the corresponding values of h, with the superscripts + and − indicating the ψ_+ and ψ_- solutions. (For example, 0.2802^+ marks the branch of the ψ_+ with $h=0.2802$.) Note that as $h\to 0$, the stability domain of the ψ_- tends to $\sqrt{2}\leqslant V\leqslant 2$ and that of the ψ_+ to $0\leqslant V\leqslant\sqrt{2}$. The whole of the $h=0$ branch is stable.

IV. BIFURCATION DIAGRAM

We used a predictor-corrector continuation algorithm with a fourth-order Newtonian solver to continue solutions of Eq. (4) in V. Since derivatives of the momentum integral (10) determine stability and branching properties of solutions, the momentum was our natural choice for the bifurcation measure. Equation (4) was solved under the vanishing boundary conditions $\psi(\pm L/2)=0$. We used $L=200$ (except in cases where we had to extend the interval to account for slow decay of solutions) and the discretization step size $\Delta x=0.005$. The eigenvalue problem (7) was solved on the interval $(-50,50)$. Here we utilized the Fourier method, typically with 600 harmonics.

A. The traveling ψ_- soliton

We start our description with the branch departing from the quiescent soliton ψ_-. For every h this branch continues all the way to $V=c$, where c is the minimum phase velocity of linear waves given by Eq. (6). As $V\to c$, the decay rate of $\psi(x)$ decreases and the soliton merges with the zero solution, with the momentum P tending to zero. (See Fig. 2). For technical reasons we could not connect the curve $P(V)$ to zero although we were able to approach the value $V=c$ as close as the fourth digit after the decimal point. (The problem is that since the decay rate of the solution decreases, one has to increase the length of the integration interval—and this cannot be done indefinitely.) The only curve that is connected to zero in Fig. 2, is the one for the undriven case $h=0$. In this case we enjoy an explicit solution (11) with the momentum $P=V\sqrt{1-V^2/4}$.

For each h the momentum of the soliton has a single maximum on this branch, at $V=V_c$ (Fig. 2). To the left of V_c the linearized operator (7) and (8) has a pair of real eigenvalues $\pm\lambda$ and consequently, the soliton ψ_-, which is well

known to be unstable for $V=0$ [5], remains unstable for small nonzero velocities. As V approaches V_c, the two eigenvalues converge at the origin on the complex plane, with the associated eigenfunctions tending to the translation mode $\Psi_0'(x)$. Increasing V past V_c, the eigenvalues move onto the imaginary axis and hence the ψ_- soliton becomes stable for sufficiently large velocities (where $\partial P/\partial V<0$). This change of stability properties is in exact agreement with the scenario described in Sec. II C. It is also fitting to note that for a given value of the momentum, solutions on the stable branch have *lower* energies than solitons on the unstable branch (where $\partial P/\partial V>0$).

B. The ψ_+ soliton; $h\leqslant 0.25$

Unlike the ψ_--branch, the final product of the continuation of the soliton ψ_+ depends on the value of h. For $h<0.28$ the fate of the soliton ψ_+ is similar to that of the ψ_-. As $V\to c$, the soliton develops oscillations on its tails; the width of the resulting oscillatory ''wave packet'' grows and the amplitude decreases, until the solution becomes equal to zero everywhere. The momentum $P(V)$ tends to zero as $V\to c$ and has a single maximum at some $V=V_c$. Stability properties of the ψ_+ soliton depend on whether h is smaller than 0.064, lies between 0.064 and 0.25, or is greater than 0.25.

Let, first, $0.064<h\leqslant 0.25$. In this case the ψ_+ soliton with V zero and small has a quadruplet of complex eigenvalues in the spectrum of the linearized operator. This implies the oscillatory instability. As V is increased, both imaginary and real parts of the ''unstable'' eigenvalues decay, with the real parts decaying faster. Eventually, for V equal to some V_s, the eigenvalues $\pm\lambda,\pm\lambda^*$ converge, pairwise, on the imaginary axis and the soliton stabilizes. Increasing V still further, two of the resulting imaginary eigenvalues λ and $-\lambda$, start approaching each other. At $V=V_c$ where $\partial P/\partial V=0$, they collide and move onto the real axis. The soliton loses its stability once again—this time to a nonoscillatory mode. The unstable real eigenvalue persists in the spectrum for all $V>V_c$, i.e., in the whole region where the slope $\partial P/\partial V$ remains negative. (Note that the ψ_- was unstable for *positive* $\partial P/\partial V$.) This scenario is exemplified by the curves $h=0.1^+$ and $h=0.15^+$ in Fig. 2.

The smaller the $h\in(0.064,0.25)$, the smaller is the value of the stabilization velocity V_s. For $h\leqslant 0.064$ the oscillatory instability does not arise at all (i.e., $V_s=0$), and the entire range $0<V<V_c$ is stable. (See the $h=0.05^+$ curve in Fig. 2).

C. The ψ_+ soliton; $h>0.25$

Let now $0.25<h<0.28$, and assume we are moving along the ψ_+ branch in the direction of larger V. For small V we have a quadruplet of complex eigenvalues $\pm\lambda$, $\pm\lambda^*$ implying the oscillatory instability. As V is increased, both imaginary and real parts decay—as in the $h\leqslant 0.25$ case. However, this time the imaginary parts decay faster than the real parts, and the two pairs of eigenvalues converge on the *real* axis. For velocities above this point the oscillatory instability is replaced by the nonoscillatory one. As V is increased further, one pair of the newly born real eigenvalues grows in absolute value whereas the other pair decreases in magnitude. At the point $V=V_c$ where $P(V)$ reaches its maximum, the latter pair converges at the origin and moves onto the imaginary axis. (This does not render the soliton stable though, as the other pair remains on the real axis.) This scenario is exemplified by the curve $h=0.27^+$ in Fig. 2.

Next, let h be greater than 0.28. For these h the branch $P(V)$ emanating from the origin, turns back at some $V=V_{\max}$ (Fig. 2), with the derivative $\partial P/\partial V$ remaining strictly positive for all $V\leqslant V_{\max}$. Below we will describe the transformation this solution undergoes when continued beyond the ''turning point,'' while here we only wish to emphasize that no new zero eigenvalues can appear at this point. The reason is that $V=V_{\max}$ is a bifurcation point of solutions of the *ordinary* differential equation (4) but not of the *partial* differential equations (1)–(3). (In other words, V is an ''internal'' parameter characterizing the solution and not an ''external'' control parameter.) Indeed, the soliton is a member of a two-parameter (x_0 and V) family of solutions of Eqs. (1)–(3) and hence for *any* V there are two zero eigenvalues in the spectrum of the linearized operator $\mathcal{H}$. Consequently, despite being a turning point for the ODE (4), the value $V=V_{\max}$ is no special as far as the PDE (1)–(3) and its linearization are concerned. No changes of the soliton's stability properties occur at this velocity.

How does one type of behavior of the curve $P(V)$, occurring for $h>0.28$, replace the other one, arising for $h<0.28$? We scanned the interval $0.280\,00<h<0.280\,20$ and discovered a tiny region of transitional behavior, around $h=0.280\,05$. For this h, $P(V)$ grows until it reaches a maximum at $V_c=1.051$ and then starts decreasing, as in the case of $h<0.28$. However, the curve does not decay all the way to $P=0$ as would be the case for $h<0.28$, but reaches a minimum at $V_{cc}=1.0563$. After that, the momentum starts growing, and, at $V_{\max}=1.0565$, the curve $P(V)$ turns back—just like for $h>0.28$! To get an idea of how small this window of transitional behavior is, it suffices to say that for $h=0.280\,00$ the momentum $P(V)$ decays to 0 as $V\to c$, whereas for h as close as $0.280\,10$, the curve $P(V)$ already has a ''turning point,'' with P continuing to increase all the time.

What happens to the ψ_+ soliton with $h>0.28$ (more precisely, with $h\geqslant 0.28010$) as we continue it beyond the turning point? Figure 3 shows the momentum as a function of V. The point of intersection with the vertical axis $V=0$ corresponds to the twist solution [Eq. (19) with $z=\zeta$ given by Eq. (22).] In Fig. 3, it is marked as ψ_T. Since the $V=0$ twist is a representative of a two-parameter family of stationary solutions of Eq. (3), there should be four zero eigenvalues in the spectrum of the operator $\mathcal{H}$ in this case, with two linearly independent eigenfunctions given by $\partial_x\Psi(z;x)|_{z=\zeta}$ and $\partial_z\Psi(z;x)|_{z=\zeta}$. [Here $\Psi(z;x)$ is a two-component vector formed by the real and imaginary parts of Eq. (19).] Numerically, we observed that as we approach the $V=0$ twist from the direction of positive V, a pair of opposite eigenvalues converges at the origin on the complex plane. The curve

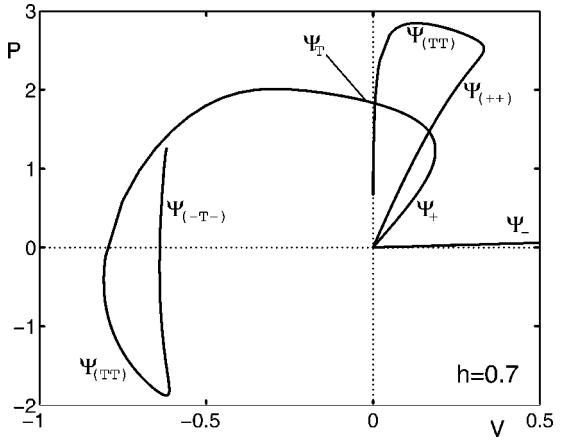

FIG. 3. The full bifurcation diagram for $h=0.7$. All branches shown in this figure are unstable. (For $h=0.7$ the soliton ψ_- is stable at large velocities but the region of stability lies beyond the frame of this figure—see Fig. 2.) More solution branches can be obtained by the reflection $V\to -V$, $P\to -P$.

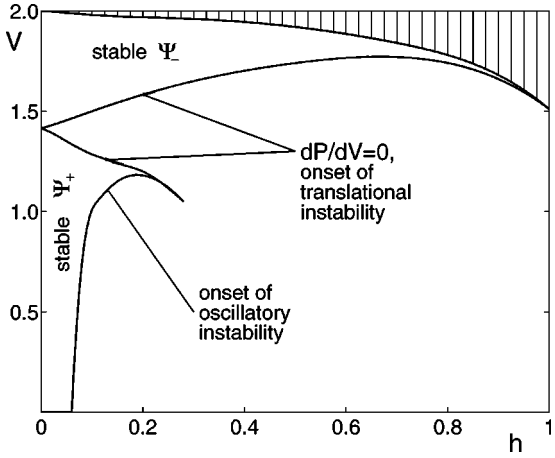

FIG. 4. Stability diagram for the ψ_+ and ψ_- solitons on the (h,V) plane. In the region marked ''stable'' one of the two one-soliton solutions is stable whereas the other one is not. Across the solid line, the corresponding soliton loses its stability to an oscillatory or monotonically growing mode. No solitons exist in the dashed region.

$P(V)$ does not have an extremum at this point and this may seem to be in contradiction with predictions of Sec. II C. The paradox is resolved as soon as one recalls that the extremality condition $\partial P/\partial V=0$ was derived under the assumption that there is only *one* eigenvector associated with the zero eigenvalue whereas we have *two* linearly independent null eigenvectors in the case at hand.

As we continue further into the region $V<0$, the twist gives rise to a variety of multisoliton complexes; we shall describe them in the next subsection. Here we will restrict ourselves to the region $V>0$ where this branch can still be regarded as a branch of one-soliton solutions. Although these solutions undergo similar transformations for all h in the interval $(0.28,1)$, there are a few differences with regard to the trajectories of eigenvalues on the complex plane. One difference worth mentioning is that for the driving strength $h=0.3$ and larger h, the quadruplet of complex λ persists on the entire upper branch of $P(V)$ (i.e., for all $V>0$). This is in contrast to the case of $0.25<h<0.28$, where the complex quadruplet converges on the real axis. Near the left end of the interval $0.28<h<1$ (e.g., for $h=0.2802$), we have an intermediate pattern. Similarly to the case $h<0.28$, here the complex quadruplet converges on the real axis somewhere on the lower branch of $P(V)$ (i.e., before the turning point), but as we move onto the upper branch, the two emerging real pairs reunite quickly and the complex quadruplet reappears.

Next, as we know, there are only two points where a pair of eigenvalues can pass from the real onto the imaginary axis, or vice versa. One point is $V=V_c$ where $\partial P/\partial V=0$, and the other one is $V=0$. Therefore the dynamics of eigenvalues depends on which of the two points comes first, or, equivalently, whether the upper branch of $P(V)$ has the maximum for positive or negative V. For smaller values of h in the interval $(0.28,1)$ (e.g., $h=0.3$), where $V_c>0$, two imaginary eigenvalues move to the real axis at $V=V_c$. These imaginary eigenvalues have detached from the continuous spectrum somewhere before the turning point [i.e., on the lower branch of $P(V)$.] The two newly born real eigenvalues first diverge from the origin but then reverse and, at $V=0$, move back onto the imaginary axis. For larger h (e.g. $h=0.7$), where $V_c<0$, the pattern is different. For these h the two imaginary eigenvalues become real not at the point V_c but at $V=0$. Subsequently, as we continue the branch to negative velocities, another pair of imaginary eigenvalues detaches from the continuum and at the point $V_c<0$ two (imaginary or real) eigenvalues pass through the origin.

Figure 4 shows the stability diagram of the ψ_+ and ψ_- solitons on the (h,V) plane. For the ψ_+ soliton, the range of stable velocities approaches $0\leqslant V<\sqrt{2}$ as $h\to 0$, while the stability range of ψ_- tends to $\sqrt{2}<V\leqslant 2$. Finally, the domain of stability in the $h=0$ case is the union of the above two ranges: $0\leqslant V\leqslant 2$.

D. Other branches; $h>0.28$

As we continue it to negative velocities, the twist (we are using this name here for $V\neq 0$ deformations of the quiescent twist solution) gradually transforms into a complex of two twists [plotted in Fig. 5(a)]. A further continuation of this branch takes us, via several ''turning points,'' to a solution that can be interpreted as an association of the twist and two ψ_- solitons of opposite polarities (denoted $\psi_{(-T-)}$). This solution is depicted in Fig. 5(b).

Another branch emanating from the origin in Fig. 3, is a bound state of two solitons ψ_+. This solution was *not* obtained by the continuation from $V=0$ as Fig. 3 may seem to be suggesting. Instead, we fixed a nonzero V and continued in h from the value $h=0.05$ where the complex $\psi_{(++)}$ arises from the V-continuation of the twist soliton (see Sec. IV E). Omitting details of this procedure, we start the description of the resulting branch at some point (V,P) away from the origin. As we approach the origin from this point, the separation between the solitons ψ_+ in the complex $\psi_{(++)}$ rapidly increases so that the field values between the two solitons

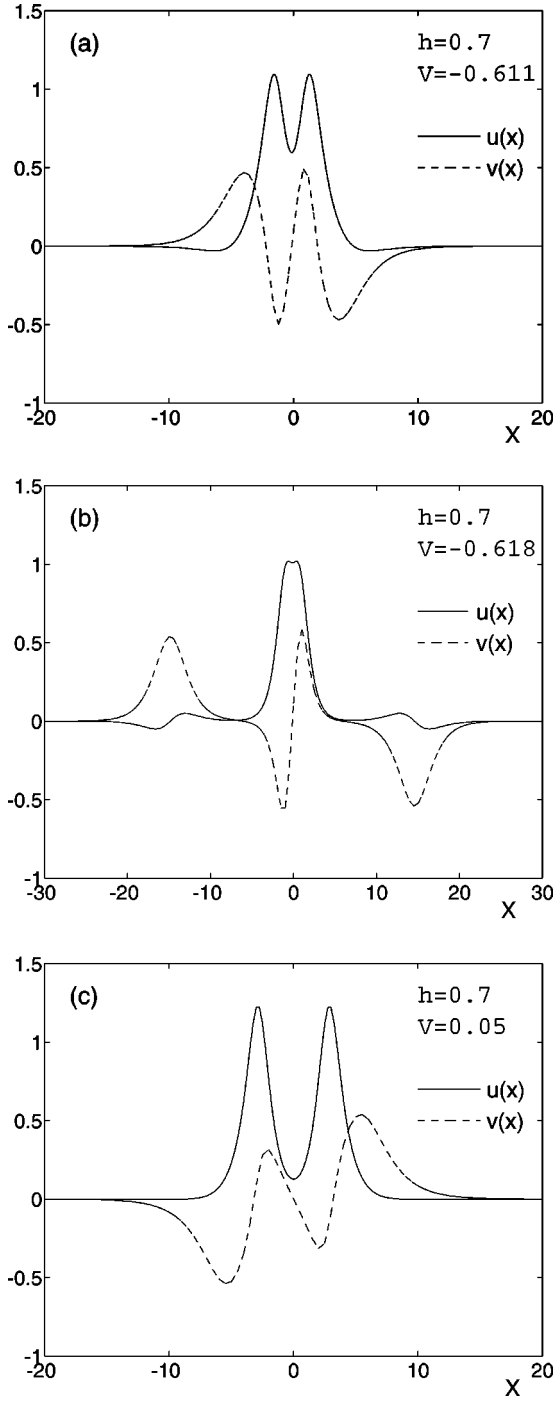

FIG. 5. (a) The $\psi_{(TT)}$ complex. (b) The $\psi_{(-T-)}$ solution. (c) A complex of two twist solitons arising from the continuation of the $\psi_{(++)}$ bound state. [Note the difference from the other two-twist complex shown in (a).] Solid line: real part; dashed line: imaginary part.

become exponentially small. For example, for $h=0.7$, the (numerically calculated) separation at the point $V=0$ was equal to $z\approx 21$. The value of $|\psi|$ at the point on the x axis, equally distanced from the left and right soliton, was of order 10^{-6}. Consequently, the nonlinear term in the Eq. (4) becomes negligible away from the solitons' core and, in spite of an extremely small value of the residual that we used in

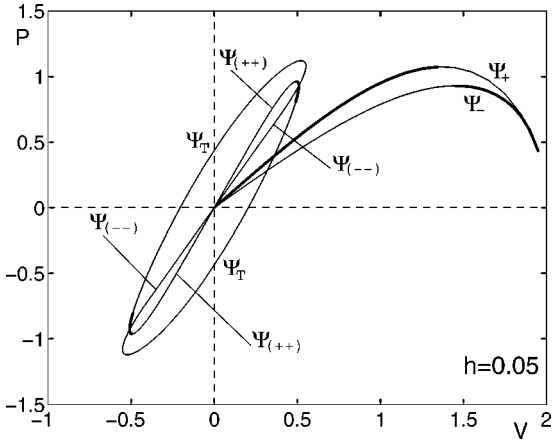

FIG. 6. The full bifurcation diagram for $h=0.05$. Thick and thin lines depict stable and unstable branches, respectively. Note a region of stability of the complex $\psi_{(++)}$. Additional branches can be generated by employing the reflection symmetry $V\rightarrow -V$, $P\rightarrow -P$.

our numerical algorithm (10^{-10}), we were unable to distinguish between a genuine bound state and a linear superposition of two distant solitons. We *conjecture* that the complex $\psi_{(++)}$ exists all the way to $V=0$ but as $V\rightarrow 0$, the intersoliton separation $z\rightarrow\infty$. Another indication to this effect is that as $V\rightarrow 0$, the imaginary part of the solution tends to zero, rapidly and uniformly. Since the only pure real solution that exists for $V=0$ is the (single) soliton ψ_+, the $V\rightarrow 0$ limit of the $\psi_{(++)}$ complex should be an infinitely separated pair of the ψ_+'s.

If we, conversely, continue our solution away from the origin, the curve $P(V)$ turns left at some V and the complex $\psi_{(++)}$ transforms into what can be interpreted as a bound state of two twists (denoted $\psi_{(TT)}$ in Fig. 3.) This solution is depicted in Fig. 5(c). As $V\rightarrow 0$, the momentum of this bound state tends to zero (Fig. 3). Unfortunately, we were only able to obtain this solution away from some small neighborhood of $V=0$. (For $h=0.7$, the smallest value of the velocity for which we were still able to find the solution in question, was $V=0.000\,283$.) Whether this branch can be continued to $V=0$, remains an open question.

E. Other branches; $h<0.28$

As we have mentioned, for $h<0.28$ the branch ψ_+ extends all the way to $V=c$ where it merges with the zero solution. No other solutions can be obtained from the ψ_+ soliton. However, in this case we can obtain new branches by continuing the (quiescent) twist soliton, Eq. (19) with $z=\zeta$.

The resulting bifurcation diagram is shown in Fig. 6. It is convenient to start its description with the motionless twist solution with the *negative* momentum. As we move in the direction of positive V, the twist gradually transforms into a bound state of two ψ_+ solitons. At some $V=V_{max}$ the branch turns back, shortly after which, at the point $V=V_c$, the momentum reaches its maximum and starts decreasing. Adjacent to the turning point is a small range of velocities V_c

$\leqslant V \leqslant V_{max}$ where we have two *stable* solutions corresponding to each V. If we continue the branch with positive-momentum twist solution, also in the direction of positive V, the solution gradually transforms into a complex of two ψ_- solitons. The momentum reaches its maximum, starts decreasing, then the branch turns back in V and we find ourselves approaching the origin on the (V,P) plane (Fig. 6). As we move towards the origin along the $\psi_{(++)}$ or along the $\psi_{(--)}$ branch, the separation between two solitons constituting the corresponding complex grows while the imaginary part of the solution tends to zero. Similarly to what we had for larger h (Sec. IV D), we conjecture that the separation becomes infinite at $V=0$ in both cases.

Similarly to the case of large h (Fig. 3), the energy of the stable branch of ψ_- is lower than the energy of the unstable branch. The bound states on the stable $\psi_T \to \psi_{(++)}$ branch also have lower energies than their counterparts with the same P and smaller $|V|$. However, in the case of the ψ_+ solitons we have an interesting reverse of fortunes: out of the two branches with the same P, the stable branch is the one with the *higher* energy.

V. NONLINEAR STAGE OF INSTABILITY

In this section we present results of our numerical simulations of the full time-dependent nonlinear Schrödinger equation (2). The objective was to study the nonlinear stage of the development of instabilities reported in the previous section and to identify the attractors emerging as $t \to \infty$. We utilized a split-step pseudospectral method, with $2^{11}=2048$ modes on the intervals $-40 \leqslant X \leqslant 40$ and $-80 \leqslant X \leqslant 80$, and with $2^{12}=4096$ modes on the interval $(-60,60)$. The method imposes periodic boundary conditions $\psi(L/2,t) = \psi(-L/2,t)$, $\psi_X(L/2,t)=\psi_X(-L/2,t)$.

We have simulated the evolution of moving solitons unstable against an oscillatory mode and those with a positive, nonoscillatory, eigenvalue in their linearized spectrum. One of our conclusions here is that both types of instabilities give rise to the same asymptotic attractors. (This is in agreement with earlier simulations of motionless solitons [13].)

A. The decaying breather

Depending on the value of the driving strength, the initial conditions and the choice of the parameters of the numerical scheme, we observed one of the two scenarios. In the first scenario the soliton transforms into a bell-shaped structure, with a small amplitude and large spatial width, oscillating approximately as $\psi \sim e^{i\omega t}$, with *negative* ω. This localized solution was previously encountered in numerical simulations of Ref. [13] where it was termed *breather*. The amplitude of the breather slowly decays with time and the width slowly grows.

We have detected this scenario for the driving strength $h=0.1$, with the initial condition in the form of the ψ_+ soliton traveling with the velocity $V=0.05$ and with $V=0.8$. (For both values of the velocity the ψ_+ soliton is unstable against an oscillatory mode.) Unlike earlier simulations [13] that started with the initial condition in the form of a quiescent unstable soliton and gave rise to a quiescent breather, the breather emerging from a traveling soliton has a nonzero speed.

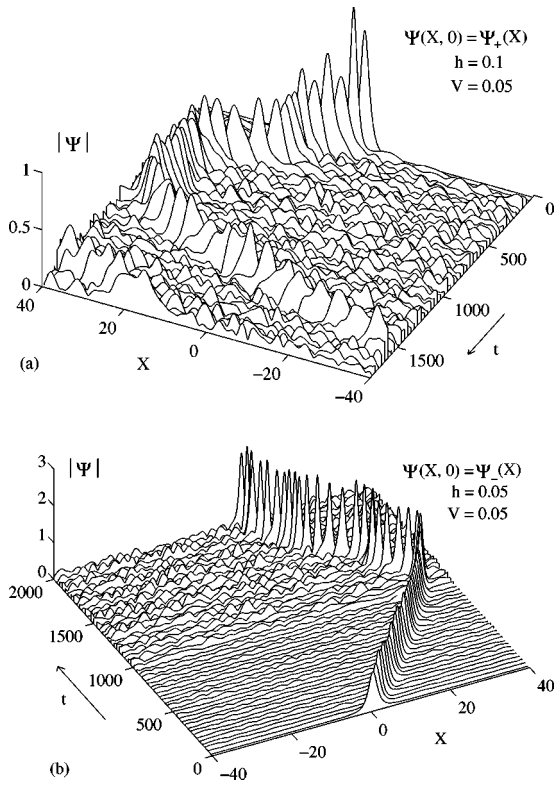

FIG. 7. The two types of asymptotic attractors resulting from the decay of the unstable steadily traveling solitons: (a) the decaying and (b) the growing breather. (a) corresponds to $h=0.1$ and the initial condition in the form of the ψ_+ soliton with $V=0.05$. In (b), $h=0.05$ and the initial condition was chosen as the ψ_- soliton with $V=0.05$. In both plots the emerging breather changes, spontaneously, its direction of motion. (Note that this happens *not* as a result of the reflection from the boundary, as the periodic boundary conditions are imposed.)

One may naturally wonder whether the speed of the breather will decay to zero or approach a nonzero constant value as t increases. Our simulations seem to support the latter hypothesis. In one run, the speed of the breather evolving out of the soliton traveling with the initial velocity of $V=0.05$, was seen to slowly grow and gradually approach the constant value of 0.1. This simulation was repeated, with the same parameters of the numerical scheme and an initial condition that was only different from the previous one due to interpolation errors of order 10^{-6}. In this run the breather was first seen to slow down, stop but then start moving in the opposite direction with the velocity close to -0.2; see Fig. 7(a). (This remarkable sensitivity to the initial data deserves a separate comment; see below.) The velocity of the breather evolving out of the $V=0.8$ soliton, was tending to approximately 2.1. However, for large t the unambiguous interpretation of the numerical data is hindered by the growth of the amplitude of the radiation background. The radiation waves emitted by the oscillating breather reenter the interval via the periodic boundary conditions and at a certain stage their am-

plitudes become comparable with the amplitude of the breather. Consequently, the constant-velocity motion of the breather may have been induced by the interaction with the background radiations.

B. The growing breather

The decaying breather was detected in simulations on the interval $(-40,40)$ with $N=2^{11}$ modes. However, for the same value of the control parameter ($h=0.1$) and the same initial conditions ($V=0.05$ and $V=0.8$), changing just the parameters of the numerical scheme produced an entirely different scenario.

Namely, we increased the number of the Fourier modes to $N=2^{12}$ and the length of the interval first to $L=120$ and then to 160. As in the case of $L=80$ and $N=2^{11}$, in simulations with the new values of N and L the unstable traveling soliton ψ_+ was seen to transform into a bell-shaped structure, oscillating roughly as $\psi \sim e^{i\omega t}$. However, this time the emerging breather has a *positive* frequency ω; its amplitude is large and continues to slowly grow, while the width is narrow and keeps on decreasing [Fig. 7(b)].

This attractor was also observed previously in [13]. It was found there that the decaying and growing breather coexist. Whether the evolution of the same unstable soliton settles to one or the other asymptotic attractor, was found to depend on the choice of the phase of a small perturbation applied to the initial condition. In our present simulations, the perturbation is modified simply by changing the parameters of the numerical scheme.

We also examined initial conditions in the form of translationally unstable solitons, including the ψ_+ soliton with $V=1.4$ for the driving strength $h=0.1$ and the ψ_- soliton with initial velocities $V=0.05$ and $V=1.4$, for the driving strength $h=0.05$. For each of the above three situations the simulations were repeated with 2^{11} modes on the interval $-40 \leqslant X \leqslant 40$, and with 2^{12} modes on the intervals $(-60,60)$ and $(-80,80)$. In all nine runs the unstable soliton was seen to evolve into the growing breather. (Nevertheless, it is possible that some other choices of the numerical parameters may give rise to the decaying breather instead.)

The velocity of the growing breather may vary during its evolution. It can even wander erratically, changing the direction of its motion several times, but eventually, for $t \sim 10^4$ or even earlier, the speed of the breather locks on to some constant value. Since the amplitudes of radiation waves are comparable with the amplitude of the breather at that stage, this effect can be induced by the breather-radiation interactions.

VI. CONCLUSIONS

The main result of this paper is the demonstration of the existence of wide classes of traveling soliton solutions of the (undamped) parametrically driven nonlinear Schrödinger equation. We established the necessary conditions under which motionless solitons can be continued to nonzero velocities, and, in cases where these conditions were met, were indeed able to carry out the numerical continuation. As opposed to the case of the soliton ψ_-, which undergoes similar transformations for any h, the result of the continuation of the ψ_+ has turned out to be sensitive to the value of the driving strength. We have identified two different transformation scenarios, one occurring for small and the other one for larger h.

A special attention was paid to the stability of arising solutions. We have identified three stable branches. First, the quiescent soliton ψ_-, which is known to be unstable for all h [5], was shown to stabilize when traveling faster than a certain critical velocity. In a similar way the soliton ψ_+ (which is known to be unstable for $h>0.064$ while at rest [5]), may stabilize when traveling above a certain speed. The stability region on the (h,V) plane is shown in Fig. 4. For small driving strengths, stable nonpropagating and moving solitons are seen to coexist while strongly forced solitons can only be stable when moving sufficiently fast. No matter how strong is the driver (as long as $h<1$), it can always support one or two windows of stable velocities. The bound state $\psi_{(++)}$ also displays a region of stability for small h—see Fig. 6. Finally, we were distinguishing between oscillatory and translational instabilities. The onset values of the translational instabilities, obtained numerically, were shown to verify the relation $\partial P/\partial V=0$ predicted by our theoretical analysis.

ACKNOWLEDGMENTS

We thank Dmitry Pelinovsky for drawing our attention to Ref. [14] and solution (19) presented therein. Useful conversations with Yuri Gaididei are also gratefully acknowledged. Special thanks go to Nora Alexeeva for providing us with a code for the time-dependent NLS equation and helping with numerics. One of the authors (I.B.) is grateful to Professor I. V. Puzynin of the LCTA-JINR for his strong administrative support of this project during that author's visit to Dubna. I.B. was supported by the NRF of South Africa and URC of the University of Cape Town. E.Z. was supported by an RFBR Grant No.0001-00617.

[1] J.W. Miles, J. Fluid Mech. **148**, 451 (1984); M. Umeki, J. Phys. Soc. Jpn. **60**, 146 (1991); J. Fluid Mech. **227**, 161 (1991).

[2] X.N. Chen and R.J. Wei, J. Fluid Mech. **259**, 291 (1994); X. Wang, R. Wei, Phys. Lett. A **192**, 1 (1994); W. Wang, X. Wang, J. Wang, R. Wei, *ibid.* **219**, 74 (1996); X. Wang, R. Wei, *ibid.* **227**, 55 (1997); X. Wang and R. Wei, Phys. Rev. Lett. **78**, 2744 (1997); Phys. Rev. E **57**, 2405 (1998); X. Wang, J. Acoust. Soc. Am. **104**, 715 (1998).

[3] I.H. Deutsch and I. Abram, J. Opt. Soc. Am. B **11**, 2303 (1994); A. Mecozzi, L. Kath, P. Kumar, and C.G. Goedde, Opt. Lett. **19**, 2050 (1994); S. Longhi, *ibid.* **20**, 695 (1995); Phys. Rev. E **55**, 1060 (1997).

[4] V.E. Zakharov, V.S. L'vov, and S.S. Starobinets, Usp. Fiz. Nauk **114**, 609 (1974) [Sov. Phys. Usp. **17**, 896 (1975)]; M.M. Bogdan, A.M. Kosevich, and I.V. Manzhos, Fiz. Nizk. Temp.

11, 991 (1985) [Sov. J. Low Temp. Phys. **11**, 547 (1985)]; H. Yamazaki and M. Mino, Prog. Theor. Phys. Suppl. **98**, 400 (1989).

[5] I.V. Barashenkov, M.M. Bogdan, and V.I. Korobov, Europhys. Lett. **15**, 113 (1991).

[6] B. Denardo, B. Galvin, A. Greenfield, A. Larraza, S. Putterman, and W. Wright, Phys. Rev. Lett. **68**, 1730 (1992); G. Huang, S.-Y. Lou, and M. Velarde, Int. J. Bifurcation Chaos Appl. Sci. Eng. **6**, 1775 (1996).

[7] A.V. Ustinov, B.A. Malomed, and S. Sakai, Phys. Rev. B **57**, 11 691 (1998); H.S.J. van der Zant *et al.*, Physica D **119**, 219 (1998); O.M. Braun, Yu.S. Kivshar, Phys. Rep. **306**, 1 (1998); A.C. Scott, *Nonlinear Science: Emergence and Dynamics of Coherent Structures* (Oxford Univ. Press, New York, 1999).

[8] P. Coullet, J. Lega, B. Houchmanzadeh, and J. Lajzerowicz, Phys. Rev. Lett. **65**, 1352 (1990); C. Elphick, A. Hagberg, B.A. Malomed, and E. Meron, Phys. Lett. A **230**, 33 (1997).

[9] I.V. Barashenkov and V.G. Makhankov, Phys. Lett. A **128**, 52 (1988); I.V. Barashenkov, T.L. Boyadjiev, I.V. Puzynin, and T. Zhanlav, *ibid.* **135**, 125 (1989); M.M. Bogdan, A.S. Kovalev, and A.M. Kosevich, Fiz. Nizk. Temp. **15,** 511 (1989) [Sov. J. Low Temp. Phys. **15**, 288 (1989)]; Yu.S. Kivshar and X. Yang, Phys. Rev. E **49**, 1657 (1994).

[10] I.V. Barashenkov and E.Yu. Panova, Physica D **69**, 114 (1993).

[11] I.V. Barashenkov, Phys. Rev. Lett. **77**, 1193 (1996).

[12] D.E. Pelinovsky, Yu.S. Kivshar, and V.V. Afanasjev, Phys. Rev. E **54**, 2015 (1996).

[13] N.V. Alexeeva, I.V. Barashenkov, and D.E. Pelinovsky, Nonlinearity **12**, 103 (1999).

[14] M.V. Tratnik and J.E. Sipe, Phys. Rev. A **38**, 2011 (1988).

[15] I.V. Barashenkov, E.V. Zemlyanaya, and M. Bär, report nlin.PS/0010008 (unpublished); also available as the JINR preprint E17-2000-147, Dubna (2000) and the preprint mpipks/0009011 of the Max-Planck-Institut für Physik komplexer Systeme, Dresden (2000) (unpublished).